

RSC Advances



This is an *Accepted Manuscript*, which has been through the Royal Society of Chemistry peer review process and has been accepted for publication.

Accepted Manuscripts are published online shortly after acceptance, before technical editing, formatting and proof reading. Using this free service, authors can make their results available to the community, in citable form, before we publish the edited article. This *Accepted Manuscript* will be replaced by the edited, formatted and paginated article as soon as this is available.

You can find more information about *Accepted Manuscripts* in the [Information for Authors](#).

Please note that technical editing may introduce minor changes to the text and/or graphics, which may alter content. The journal's standard [Terms & Conditions](#) and the [Ethical guidelines](#) still apply. In no event shall the Royal Society of Chemistry be held responsible for any errors or omissions in this *Accepted Manuscript* or any consequences arising from the use of any information it contains.

Molecular Effects of Encapsulation of Glucose Oxidase Dimer by Graphene[‡]

Umesh Ghoshdastider^{a,‡,§}, Rongliang Wu^{a,‡,§}, Bartosz Trzaskowski^b, Krzysztof Mlynarczyk^b, Przemyslaw Miszta^b, Manickam Gurusaran^c, Sowmya Viswanathan^d, Venkatesan Renugopalakrishnan^c, and Slawomir Filipek^{b,*}

^a Laboratory of Biomodeling, International Institute of Molecular and Cell Biology, ul. Ks. Trojdena 4, 02-109 Warsaw, Poland

^b Laboratory of Biomodeling, Faculty of Chemistry & Biological and Chemical Research Centre, University of Warsaw, ul. Pasteura 1, 02-093 Warsaw, Poland

^c Children's Hospital, Harvard Medical School, Center for Life Sciences, 3 Blackfan Circle, Boston, MA 02115, USA

^d Wellesley Hospital/Partners Healthcare System, 2014 Washington St, Newton, MA 02462, USA

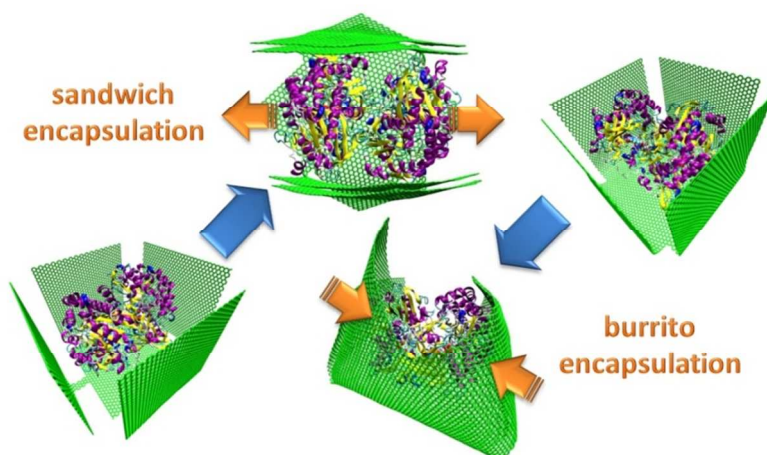
[‡] These authors contributed equally.

Corresponding Author

* Slawomir Filipek, sfilipek@chem.uw.edu.pl

Table of Contents entry

Employing boxlike shape of graphene leads to different types of “sandwich” or “burrito” encapsulation of the enzyme. To preserve the critical interactions in the enzyme active site a proper balance of forces between protein and graphene is required.



Abstract

Knowing the nature of enzyme-graphene interface is critical for a design of graphene-based biosensors. The extensive contacts between graphene and enzyme could be obtained by employing a suitable encapsulation which does not impede its enzymatic reaction. We have performed molecular dynamics simulations to obtain an insight on many forms of contact between glucose oxidase dimer and the single-layer graphene nano-sheets. The unconnected graphene sheets tended to form a flat stack regardless of their initial positions around the enzyme, whereas the same graphene sheets linked together formed a flower-like shape engendering different forms of wrapping the enzyme. During the encapsulation no core hydrophobic residues of the enzyme were exposed. Since the polar and charged amino acids are populated the enzyme's surface we also estimated, using DFT calculations, the interaction energies of individual polar and charged amino acid residues with graphene. It was found that the negatively charged residues can bind to graphene unexpectedly strongly, however, the main effect of encapsulation comes from the overlap of adjacent edges of graphene sheets.

1. Introduction

Enhanced sensitivity, improved response time and a smaller size of carbon nanomaterials makes them more suitable than traditional materials for biosensors and other applications.¹⁻³ Graphene, a single monolayer of graphite, is a two-dimensional nanomaterial which is finding numerous applications in nanoelectronics, photovoltaics and chem/bio-sensing.⁴ Graphene is phenomenally strong, flexible, transparent and a highly conductive material. Nowadays, graphene can be fabricated in many shapes and sizes,⁵ via chemical vapour deposition,⁶ horizontally grown in lithographically patterned hexagonal boron nitride atomic layers,⁷ or as freestanding vertical graphene sheets grown on a copper foil,⁸ which together with its large surface area makes it advantageous for many applications. Graphene-based devices have a lower resistance and about three orders of magnitude smaller noise amplitude than those based on nanotubes.⁹ Furthermore, the robust nature of sp²-bonded carbons forming a honeycomb lattice makes graphene chemically stable and biocompatible.^{10, 11} Hence, graphene could be relatively advantageous for specific applications (e.g. biosensing) compared to other carbon nanomaterials.^{2, 12} In addition, the zero-band gap of pristine graphene can be very useful for the construction of highly sensitive sensors even for label-free single-molecule detection.¹³ Glucose oxidase (GOx) is a glycoprotein that catalyses the oxidation of β -D-glucose to δ -gluconolactone and hydrogen peroxide in the presence of oxygen (Fig. 1). The presence of glucose in blood plasma could be detected by a change in the potential of an electrode adjacent to GOx during catalysis of glucose.¹⁴ The oxidation overpotential of the electrode reaction can be reduced by modifying the electrode with graphene or carbon nanotubes (CNT), which facilitate a direct electron transfer from the GOx active site.¹⁵ Apart from GOx many other enzymes, such as horseradish peroxidase,¹⁶ cholesterol oxidase,¹⁷ cytochrome P450, glutamate dehydrogenase or lactate dehydrogenase,^{18, 19} were used in the biosensor development.

Nanomaterials for biomedical applications have been intensively investigated, especially graphene based^{20, 21} and mixed graphene/CNT.²² However, there are nearly no studies revealing the details of graphene-enzyme interactions and how the specific graphene shape can modify the enzyme structure and function. In this paper, we have performed the all-atom molecular dynamics (MD) simulations to study the structural fluctuations of GOx dimer and the cofactor FAD (flavin adenine dinucleotide) environment upon binding to graphene sheets in different

arrangements. We have examined a single graphene sheet, a stack of them and also a flower-like (or boxlike) graphene, which were able to establish a tight contact with the enzyme. In the course of our study, we found that the broad linkers between sheets in the flower-like graphene provided the best coverage of the protein surface resulting in a nearly complete wrapping of the enzyme. Similar shapes were investigated in the case of small cargo molecules like water²³ and hydrogen²⁴ but for proteins, there are additional difficulties concerning the stability of the protein as well as preservation of enzyme activity. For instance, the entrance for the substrate must stay open (Fig. 1b) and not be hidden by the folded graphene, hence encapsulation should not be complete.

Our MD simulations demonstrate for the first time, the process of encapsulation of a large enzyme by the graphene sheets and allow to observe the influence of encapsulation on the protein structure. Using DFT (density functional theory) calculations we also estimated the energies of binding of charged and hydrophilic residues to graphene. Such amino acids populate the enzyme surface and provide the largest contribution to the graphene-enzyme complex stability. Recently, it has been found, employing MD simulations, that the graphene sheets arranged in a boxlike structure can be used for hydrogen storage since such system provides the highest hydrogen storage density of 9.5 % H₂ weight.²⁴ The graphene sheets in this box were mended together using hydrogenation-assisted processes. Such procedure is similar to ours, since we use the widest linkers, equal to the sheet's size, to obtain a nearly complete encapsulation. However, such encapsulation can lead to distortion of protein structure, especially for dimers and higher oligomers, and to partial impairment of enzymatic activity.

2. Computational Procedures

2.1. Preparation of GOx dimer structure

For investigations of GOx-graphene interactions, we chose *Penicillium amagasakiense* glucose oxidase. It crystallized as a dimer at high resolution 1.8 Å (PDB id: 1GPE).²⁵ Each of the 64 kDa monomer chains consists of 587 amino acids. GOx from *Penicillium amagasakiense* bears 65%

sequence identity to *Aspergillus niger* glucose oxidase and their RMSD (root mean square distance) values on backbone atoms differ by only 0.7 Å. Before modelling procedures, all sugar groups were removed and missing hydrogen atoms were added using YASARA 13.8 (YASARA Biosciences Inc.).

2.2. Simulations of GOx dimer with unconnected graphene sheets

Before MD simulations the individual graphene sheets, 7 nm x 7 nm in size, were positioned close to each of the four non-identical surfaces of GOx dimer. The OPLS-AA (Optimized Potentials for Liquid Simulations - All Atom) force field was applied.²⁶ The partial charges for carbon atoms in graphene were set to zero. Non-bonded parameters for graphene correspond to those of fusion carbon atoms in naphthalene. The obtained structures of GOx-graphene complexes were placed in periodic boxes 12 nm x 12 nm x 12 nm in size and solvated with water. No FAD was included in these simulations. Counterions were added to neutralize the system. The SPC (Single Point Charge) model was used for water as this model is most suitable for the OPLS force field.²⁷ The system was equilibrated in two steps: 100 ps MD using isochoric-isothermal (NVT) ensemble followed by 1 ns MD using isothermal-isobaric (NPT) ensemble with strong harmonic restraints on the backbone atoms of the protein (force constant 100 MJ mol⁻¹ nm⁻²). Then the production MD without any restraints was carried out for 100 ns.

For all the above simulations, the short-range non-bonded interactions were cut off at 1.0 nm and long-range electrostatics was calculated using the fourth order Particle Mesh Ewald (PME) method.²⁸ Temperature was coupled by Velocity rescaling (V-rescale)²⁹ algorithm which follows the Berendsen thermostat³⁰ with an extra stochastic term to reproduce a proper canonical ensemble. Initial velocities of atoms were assigned by Maxwell distribution at 300 K. All simulations were conducted at constant temperature 300 K and 1 bar pressure. Bonds were constrained using LINCS algorithm to employ a 2 fs time step in all simulations.³¹ The Parrinello-Rahman isotropic pressure coupling was implemented for constant pressure simulations.³² All simulations were performed using Gromacs v4.5.5.^{33, 34}

2.3. Simulations of GOx dimer in graphene boxes

Squared graphene sheets of 7 nm x 7 nm were aligned to form an open boxlike structures. The bottom sheet was connected to the four surrounding sheets using one linker to each sheet. The linkers were 1.2 nm long (5 benzene rings) and four different widths were used starting from 0.7 nm (3 benzene rings) in Box1 model, 1.9 nm in Box2, 3.8 nm in Box3 and 7.0 nm (equal to the size of the sheet) in Box4. The Amber03 force field³⁵ was used for GOx and the General Amber Force Field (GAFF)³⁶ was employed for FAD. Reduced form of FAD was added to observe the influence of encapsulation on the interactions in the enzyme's active site. The structures were further energy minimized for 5000 steps, and then a 100 ps stochastic dynamics (SD) simulations were performed under constant volume with the positions of heavy atoms in GOx and FAD constrained by a force constant of $1000 \text{ kJ mol}^{-1} \text{ nm}^{-2}$. To move graphene sheets closer to GOx, a pulling force with a force constant of $1000 \text{ kJ mol}^{-1} \text{ nm}^{-2}$ was imposed on the centres of mass of opposite graphene sheets. After 100 ps all four surrounding sheets were in contact with GOx and then another 2 ns SD simulation was performed with the protein constrained and without any external forces. During this simulation the graphene sheets not only wrapped around GOx, but also overlapped with the adjacent sheets to a large extent.

To study the stability of the obtained complexes, the systems with the narrowest (Box1) and the widest linkers (Box4) were additionally simulated without any constraints in explicit water environment to test their stability. The GOx dimer-graphene complexes were soaked in water and counterions were added randomly replacing some water molecules to neutralize the system. Then, 2 ns MD simulation using NVT ensemble was performed with the positions of heavy atoms in GOx, FAD and graphene constrained to equilibrate the water and the ions. Further, 2 ns MD simulation under NPT ensemble was performed with the same constraints to equilibrate the water density. Following that, the restraints on graphene were removed and another 2 ns simulation was performed. Finally, all restraints were removed and MD runs of 100 ns were performed under NPT ensemble with all bonds constrained with the LINCS algorithm.³¹ Time step of 2 fs was used. During all MD simulations the van der Waals interaction potentials were shifted to 0 within a range 0.8-1.2 nm with the long range dispersion corrections to both energy and pressure. The long range Coulomb interactions between partial charges of atoms were calculated by the PME method with cutoff of 1.2 nm.²⁸ The temperature of the system was coupled separately for the solute and water/ion groups to a heat bath of 300 K using the Nose-

Hoover method.^{37,38} The pressure was constant at 1 bar using isotropic coupling in the Parrinello-Rahman method.³² The simulations were performed using Gromacs v4.5.5 MD simulation package.

2.4. DFT calculations

The initial geometry optimization of the graphene sheet was carried out using the SCC-DFTB method (Self-Consistent Charge Density Functional Tight-Binding)^{39,40}, as implemented in the DFTB+ software,⁴¹ and a single-layer graphene model consisted of 112 carbon atoms in a periodic box. Amino acids were modelled as all-atom side chains terminated with a CH₃ group. Glutamic acid and aspartic acid were both modelled as a glutamic acid side chain, while glutamine and asparagine were both modelled as a glutamine side chain. For each investigated case we started from two different geometries, one parallel to the graphene surface and one perpendicular, with the functional group located close to the graphene.

Geometries from the SCC-DFTB initial optimization were used as starting points to perform M06-2X density functional⁴² calculations with a small, 3-21G* basis set. For those calculations we used a graphene model consisting of 110 carbon atoms terminated with hydrogen atoms. After obtaining the geometry convergence we switched to a smaller graphene model consisting of 58 carbon atoms terminated with hydrogen atoms and used the same M06-2X method with a larger basis set 6-31+G(d,p) with diffuse functions to perform the final geometry optimization. For the M06-2X/6-31+G(d,p) level of theory, we also added a counterpoise correction to remove the basis-set superposition error.

Images were generated using YASARA⁴³ and VMD⁴⁴. MD trajectory analysis was done using Gromacs tools, VMD and custom scripts. Plots were constructed using Grace Software.

3. Results

3.1. Unconnected graphene sheets

Initially, we performed 100 ns all-atom MD simulations of GOx dimer in contact with a single graphene sheet, 7 nm x 7 nm in size, in water environment. The sheet was placed at different sides of the GOx dimer in each simulation. Only in one case, we witnessed a significant movement of graphene associated with a partial wrapping of GOx. The GOx structure stabilized after about 50 ns, however, the movement of graphene continued until the optimal contact was established after about 70 ns. Such movement was facilitated by the small area of contact, about 30 nm², and stiffness of the individual graphene sheets. The N-terminus of GOx and its flexible loops changed their conformation to establish a better contact with the graphene surface.

In the next step we used four unconnected graphene sheets located initially in the same positions as in the simulations with a single sheet (Fig. 2a) and performed 100 ns MD simulation of GOx dimer in water environment. During the simulation, after about 2 ns, three graphene sheets slid together, forming a bent stack (Fig. 2b). Then, this stack gradually flattened and after about 4 ns it moved toward the fourth graphene sheet (Fig. 2c). All these changes were accompanied by reduction of the GOx-graphene contact surface. The process of self-assembly of these highly mobile graphene sheets can be seen in Movie M1. One monomer of GOx in extensive contact with graphene stabilized after 70 ns, while the second monomer stabilized much earlier, i.e. after 30 ns (Fig. S1a†). The final graphene-protein contact involved N-terminal residues 1-9 and also some other residues from both monomers of GOx (Fig. 2c). This position proved to be stable till the end of the 100 ns simulation. Compared to the single graphene sheet in the same contact position, the protein-graphene interface diminished by 10 % from 33.5 nm² to 30.8 nm², however, the interaction became more attractive and the energy of interaction changed by 20 % from -1050 kJ mol⁻¹ to -1250 kJ mol⁻¹. Interestingly, the stack of graphene sheets adopted a flat shape and the initial curvature was lost (Movie M1). It seems that the attractive forces in a stack of just three graphene sheets were stronger than graphene interactions with the enzyme. We did not observe a large unfolding of GOx upon interaction with the flat graphene sheets. Only a small β -sheet, residues 222-229, in close contact with graphene, was unfolded. This is possibly due to a very small interacting surface between GOx and graphene and the compactness of the GOx structure composed of many extensive and hard to unfold β -sheets. Furthermore, a 7 nm x 7 nm graphene sheet may be too small to induce larger unfolding effects in such big structure as GOx dimer.

3.2. Connected sheets and encapsulation

To test the possibility of GOx encapsulation by flower-shaped graphene, we used four sheets of the same dimensions, 7 nm x 7 nm, covering each side of the GOx dimer, connected to the central graphene sheet of the same size. To connect these sheets, we employed different linkers ranging from 0.7 nm in width (three benzene rings) to 7.0 nm (equal to the size of graphene sheet): models Box1 to Box4. Performing a short 2 ns stochastic dynamics (SD) in implicit solvent, we found that the graphene sheets wrapped around GOx and attracted the edges of adjacent sheets due to the strong hydrophobic interactions between overlapping graphene surfaces (Fig. 3). An attraction between the graphene sheets is especially evident in the structure with narrowest linkers (model Box1) where two adjacent sheets at each side entirely overlap (Fig. 3a and Movie M2). The overlapped area diminished by about 20% for all graphene boxes with broader linkers (Fig. 3b-d). The largest contact surface between graphene and GOx was achieved in Box4 model, the cross-like graphene, which led to “burrito” type encapsulation (Fig. 3d and Movie M3). In Box1 the stacking effect of adjacent graphene sheets was observed, compared to Stack model, but nevertheless an encapsulation was obtained (à la sandwich) leading to the high graphene-protein contact area (calculated as a buried water-accessible surface). Such contact area was the smallest for Stack model and the largest for Box4 (Table 1). Two extreme boxlike models, Box1 and Box4, were subjected to MD simulations in explicit water environment to optimize the structures and to test their stability. As indicated by the RMSD plot (Fig. S1b†) a change in the structure of GOx in Box 1 was much smaller than in Box4. In Box 1 the RMSD was about 0.33 nm for both monomers whereas in the case of Box4 it was 0.36 nm for one monomer while for the second subunit it was as high as 0.52 nm. This highly asymmetric change in GOx structure suggests the existence of very strong forces deforming and compacting the GOx dimer. Therefore, GOx-graphene contact area in Box4 model was as high as 204 nm², nearly 50 % increase compared to Box 1, and a distance between GOx monomer centres was the shortest also for Box4 (3.24 nm). Compared to the crystal structure, this distance was shorter in Box 4 but longer in the Stack and in Box1, which indicates elongation of the GOx dimer when crystal packing forces are vanished. The contact surface between GOx monomers is much larger in Box4 compared to every other case. In the stacked configuration this GOx-GOx contact area is smaller than in the crystal structure while in Box1 it

is slightly larger. The FAD-graphene closest distance is nearly the same in Box1 and Box4, indicating that a complete wrapping does not help in bringing FAD to graphene. The GOx-graphene contact area exhibits the highest difference between Stack, Box1 and Box4 cases. For the stacked configuration the contact area is the smallest, only 31 nm², in Box 1 - 138 nm² but in Box 4 - 204 nm², indicating high degree of encapsulation. The calculated curvature of graphene in Box4 is small and nearly the same on the whole surface except for the two tightly rolled endings (Fig. 3e,f) which are similar to carbon nanotubes and approach the maximal rigidity of graphene.^{45, 46}

3.3. Structural changes of GOx

The distance between the centres of the two GOx monomers did not change during 100 ns MD simulation in Box1 while it was decreasing in the Box4 model (Fig. S2a†). In the crystal structure of GOx dimer this distance is 3.85 nm and is between the values of Box1 and Box4, indicating that GOx dimer in Box1 is elongated while in Box4 compressed. The closest distance between the cofactor FAD and graphene was diminishing in Box1 but increasing in Box4. In both cases, it reached about 1.85 nm (Fig. S2b†). A compression of GOx dimer in Box4 was rather a rounding of the shape since the volume of GOx dimer was nearly the same in Box1 and Box4, about 195 nm³. Fluctuations in volume diminished after about 50 ns in Box1 while in Box4 they were large, nearly till the end of the simulation (Fig. S3†) suggesting rather big changes in internal GOx structure during compression (i.e. rounding) that occurred in Box4 especially in monomer B (Fig. S1b†).

Root mean square fluctuations (RMSF) of residues in the individual monomers of GOx dimer indicate that in Box1 and Box4 the residues anchoring FAD (E55, N111-S114, and V254) as well as the catalytic residues (H520 and H561) are located in regions of small fluctuations (Fig. S4†). This, however, does not mean that the cofactor FAD was unmoving – especially a flavin group. Reduced form of this group, which was used in our calculations, is located nearly in the same position as oxidized form, but one hydrogen bond to G112 is lost due to protonated nitrogen in the central flavin ring (Fig. 4a). In the Box 1 model, after 100 ns of MD simulation, the catalytic residues, H520 and H563, are still located above flavin group likely to bind substrates, while carbonyl groups of the flavin ring are still bound to main chain of S114 and

M565 (Fig. 4b). Conversely, in Box4 model, the catalytic residues are found on both sides of the flavin rings (Fig. 4c) which precludes the catalytic function of such altered active site.

Such location of histidine residues is a result of a movement of the flavin group so its interactions with residues S114 and M565 are also lost. Abnormal location of catalytic residues was found in both monomers of Box4, although only one of them exhibited considerably increased RMSD values (Fig. S1b†). In all models a position of adenine part of FAD was not changed. We also compared changes in the secondary structure of monomers A and B in GOx dimer-graphene complexes of Box1 and Box4 (Fig. S5†). There was a small decrease in the α -helix content in Box1 and a large decrease by 10 % in Box4. Nearly no change of the β -sheet content was found in Box1 and Box4. In order to distinguish the conformational changes of GOx dimer in Box1 and Box4 models, we conducted the Principal Component Analysis. The movements of graphene and GOx dimer proved to be strongly correlated, especially in the case of Box4 (Fig. 5a). We also projected the trajectory of the Box4 model into Box1 along the principal components, PC1 and PC2, to compare them and to detect a phase space overlap. They overlapped only in a small region (Fig. 5b). This indicates distinct conformational changes of the GOx dimer: elongation in Box1 and compaction with rounding of the shape in Box4.

3.4. GOx-graphene interaction energy

The surface of GOx as that of other enzymes is populated mostly by polar and charged residues and its interaction with graphene, even in an encapsulated form, does not change it. Some of these residues were found to be actively contributing to the GOx-graphene interaction energy. The individual contributions of particular residue types to the interaction energy are shown in Fig. S6.† During the course of MD simulations the interaction energies for all amino acids were becoming more negative (more attractive interactions). In both Box1 and Box4 the most contributing residue types were Lys (20 residues) and Gln (13 residues) since they are the most numerous residues on the GOx surface. Nevertheless, they were also the most contributing residues when the interaction energy was normalized (divided by the number of residues of this type in contact with graphene). In Box 4, the interaction energy of these residues was about 50 % higher compared to Box1. This is because during compacting of GOx in Box4 the structure is

changing and the surface residues are interacting with graphene not only with their functional groups but also the hydrophobic part of side chains.

To more accurately estimate the effect of graphene binding by charged and polar residues, we calculated the interaction energies (E_{int}) of some hydrophilic and charged amino acids, populated the GOx surface, using DFT methods at different levels of theory. We employed the empirical exchange-correlation functional M06-2X.⁴² The interaction energy calculations included optimization of the system structure. It was found that a flat orientation of residues on the graphene surface was optimal for all analysed amino acid residues (Fig. S7†). Such geometry is favoured due to a large number of weak van der Waals interactions between the graphene sheet and the aliphatic parts of the amino acid residues since each methylene group contributes approximately 6 kJ mol⁻¹ to the interaction energy. However, the main component of the large affinity of polar and charged residues towards the graphene sheet comes from the interactions of their functional groups with the conjugated π system of the graphene. Hence, the positively charged amino acids, Lys and Arg, were characterized with the lowest interaction energy (E_{int}) values indicating the most attractive interactions.

To obtain the most accurate estimation of E_{int} for different residues we used a large basis set, 6-31+G(d,p), with the counterpoise correction. The interaction energies of side chains of polar amino acids with the graphene sheet were the following: Arg⁺: -138 kJ/mol, Lys⁺: -127 kJ/mol, Glu⁻/Asp⁻: -49 kJ/mol, Gln/Asn: -39 kJ/mol, and GluH/AspH: -38 kJ/mol. In all cases the negative values were obtained indicating that the residues were attracted by graphene. The strongest attractive forces were obtained for positively charged amino acids, however, the negatively charged residues were also attracted.

4. Discussion

The molecular dynamics studies have revealed the feasibility of efficient encapsulation of GOx by a flower-like graphene. Nearly a complete encapsulation of the enzyme (in Box4 model) led to distortions of enzyme structure and incorrect orientation of the cofactor, FAD, towards the

GOx catalytic residues. Furthermore, such extensive encapsulation could block an access of the substrate to the active site of the enzyme. However, such wrapping may be useful for rigid cargo, like quantum dots. On the other hand, using another flower-like shape of graphene in Box1 model, we obtained a stacking effect, where two stacks were created on both sides of the GOx dimer leading to elongation of the dimer. In this model the active site of both GOx monomers remained nearly intact and the entrance of the substrate was not blocked. Experimental implementation of linked graphene sheets may be difficult so such linkers may be substituted by chemical linkers which are available and used even today. For instance the porous graphene frameworks pillared by organic linkers was created by Kumar *et al.*⁴⁷. A formation of 3D structures of directly linked graphene sheets is also possible via mild chemical reduction of graphene oxide⁴⁸ although the size cannot be precisely controlled. However, such structures are also of potential importance for protein encapsulation.

It was found for GOx immobilized on the surface of multi-walled carbon nanotubes (MWCNT) that although its catalytic activity was preserved, no direct electron transfer to the electrode could had been demonstrated.⁴⁹ Similar deduction was made by Wooten *et al.*⁵⁰ indicating that GOx molecules that were within the electron tunnelling distance from CNT were not enzymatically active toward glucose. Previous reports on the occurrence of direct electron transfer in GOx systems referred to cases involving hidden mediators, including atmospheric oxygen, which is a natural electron mediator between GOx and a modified electrode surface.^{49, 51} Recently, in a four-component system involving graphene, MWCNT, metal nanoparticles and GOx it was, nonetheless, possible to detect a direct electron transfer.⁵² It was done based on a PDDA-(polydiallyldimethyl-ammonium chloride)-capped gold nanoparticle modified graphene/MWCNT electrode. Such hierarchical nanostructure can provide a larger surface area and a more favourable microenvironment for the electron transfer. Grosse *et al.*⁵³ also obtained a remarkably large catalytic current in the GOx system by using aqueous dispersions of reduced graphene oxide and MWCNT.

A highly nanostructured carbon surface was used by Ueda *et al.*⁵⁴ in the study of physically adsorbed enzyme, bilirubin oxidase. The catalytic current was 30 times greater for such surface than that obtained in the case of a flat carbon film. Such thorn-like structures were fabricated by the UV/ozone process which generates very deep pockets in which the enzyme is nearly

surrounded by the electrode material. The bilirubin oxidase differs from GOx since it contains the copper clusters which make a direct electron transfer potentially much more efficient, it is however achieved only when such structured surfaces are utilized. To enhance a contact with the enzyme, one can employ encapsulation of enzymes by graphene (or graphene oxide). However, in the case of GOx, direct electron transfer may be hard to achieve even if a very close and tight contact between the enzyme and the electrode is established. One possible way of improving glucose sensing is to employ the highly dispersed titanium dioxide nanoclusters on reduced graphene oxide as demonstrated by Luo *et al.*⁵⁵.

The flower-like graphene has been investigated before to study the encapsulation of water nanodroplet in vacuum using MD simulations. In their study,²³ Bellido and Seminario used small flakes, about 2 nm x 1.2 nm in size, linked by extremely thin linkers of single benzene ring width. Such graphene structure folded during 200 ps of MD simulation around water molecules in vacuum. On a larger scale, it has been shown experimentally that water microdroplets containing large patches of graphene oxide and silver nanoparticles as the solute, can spontaneously form nanostructures of solute cargo wrapped by graphene oxide sheets upon drying, which leads to the nearly complete encapsulation of cargo.⁵⁶

During MD simulations, we observed an attraction between graphene and different amino acids, including hydrophilic and charged residues. Even negatively charged residues exhibited such effect, which was confirmed later by our DFT calculations for Glu⁻/Asp⁻-graphene system. The strong anion- π attractive interactions were also found by Shi *et al.*⁵⁷ for a complex of graphene and halide ions. They proposed that the quadrupole-quadrupole interactions were responsible for anion- π attraction. Their calculations⁵⁷ were made for large sheets of graphene, C₈₄H₂₄. Although this effect seems to be better manifested for larger graphene sheets, the attraction could be easily demonstrated also for a smaller graphene sheet, C₅₈H₂₀, used by us. The currently available force fields can provide qualitatively correct results as exemplified by E_{int} values estimated for individual amino acids. Thus, the obtained structures of graphene-GOx complexes seem to be well founded and the molecular dynamics methods can be employed for the estimation of the influence of graphene on the structure and function of other proteins.

5. Conclusions

Although the usage of proteins and graphene in bio-nano-devices is increasing, little is known about the molecular effects of graphene on structure and function of enzymes and receptors. A direct contact of graphene with protein may be potentially hazardous and lead to unfolding of protein by flat surface of large graphene sheet. Nevertheless, a close contact between protein and graphene is necessary for obtaining a direct electron transfer from the enzyme active site. We examined different shapes of graphene and quantified their ability to wrap the enzyme, glucose oxidase dimer. Such encapsulation leads to achieving a high contact surface with graphene, however, the preservation of structure and function of enzyme is challenging and depends on the enzyme shape and location of the substrate binding pocket. The molecular dynamic simulations revealed that a very tight wrapping of the enzyme is possible but it generates structural changes in the protein, including partial impairment of its catalytic function because of relocation of catalytic residues and cofactor. Such “burrito” type encapsulation may be useful for hard cargo. Employing another boxlike shape of graphene led to “sandwich” type encapsulation. In this case we also obtained a close FAD-graphene contact while preserving the interactions in the enzyme active site critical for redox reaction. Employing MD simulations we found that even the hydrophilic and charged residues, populating the enzyme surface, were attracted by graphene, what was confirmed by subsequent DFT calculations. Such calculations can be utilized for parameterization of currently used force fields for molecular modelling to provide the quantitatively correct protein-graphene interactions. The results reported in the present study are the first step in understanding the molecular effects occurring during encapsulation of enzymes, especially GOx dimer, by graphene sheets, which we believe would be a worthy attempt. The cross-like graphene, responsible for the most efficient encapsulation (of “burrito” type), does not require any linker between adjacent graphene sheets and could be manufactured in the near future, so our predictions on feasibility of such encapsulation and also on changes in the enzyme active site would be verified.

Acknowledgments

The research leading to these results has received funding from the European Community's Seventh Framework Program under grant agreement no. 211800. S.V. and V.R. wish to acknowledge the Rothschild Foundation for the support of the biosensor project at Children's Hospital. S.V. and V.R. dedicate this article to Varun.

Notes and references

§ Present Addresses: U.G.: Institute of Molecular and Cell Biology (A*STAR), 61 Biopolis Drive, Proteos #03-15, Singapore 138673, Singapore. R.W.: College of Material Science and Engineering & State Key Laboratory for Modification of Chemical Fibers and Polymer Materials, Donghua University, Shanghai 201620, China.

† Electronic supplementary information (ESI) available: additional figures showing details of MD simulations, analyses of protein structural changes, protein-graphene interaction energies, and movies illustrating different types of encapsulation and stacking.

1. E. Lahiff, C. Lynam, N. Gilmartin, R. O'Kennedy and D. Diamond, *Anal. Bioanal. Chem.*, 2010, **398**, 1575-1589.
2. W. Yang, K. R. Ratinac, S. P. Ringer, P. Thordarson, J. J. Gooding and F. Braet, *Angew. Chem. Int. Ed.*, 2010, **49**, 2114-2138.
3. S. Viswanathan, P. Li, W. Choi, S. Filipek, T. A. Balasubramaniam and V. Renugopalakrishnan, *Methods Enzymol.*, 2012, **509**, 165-194.
4. M. Pumera, *Mater. Today*, 2011, **14**, 308-315.
5. D. Geng, B. Wu, Y. Guo, L. Huang, Y. Xue, J. Chen, G. Yu, L. Jiang, W. Hu and Y. Liu, *Proc. Natl. Acad. Sci. USA*, 2012, **109**, 7992-7996.

6. Q. Yu, L. A. Jauregui, W. Wu, R. Colby, J. Tian, Z. Su, H. Cao, Z. Liu, D. Pandey, D. Wei, T. F. Chung, P. Peng, N. P. Guisinger, E. A. Stach, J. Bao, S. S. Pei and Y. P. Chen, *Nat. Mater.*, 2011, **10**, 443-449.
7. Z. Liu, L. Ma, G. Shi, W. Zhou, Y. Gong, S. Lei, X. Yang, J. Zhang, J. Yu, K. P. Hackenberg, A. Babakhani, J. C. Idrobo, R. Vajtai, J. Lou and P. M. Ajayan, *Nat. Nanotechnol.*, 2013, **8**, 119-124.
8. N. Li, H. W. Song, H. Cui and C. X. Wang, *Nano Energy*, 2014, **3**, 102-112.
9. A. A. Balandin, *Nat. Nanotechnol.*, 2013, **8**, 549-555.
10. C. Schmidt, *Nature*, 2012, **483**, S37.
11. W. C. Lee, C. H. Lim, H. Shi, L. A. Tang, Y. Wang, C. T. Lim and K. P. Loh, *ACS Nano*, 2011, **5**, 7334-7341.
12. J. A. Rogers, M. G. Lagally and R. G. Nuzzo, *Nature*, 2011, **477**, 45-53.
13. V. G. Kravets, F. Schedin, R. Jalil, L. Britnell, R. V. Gorbachev, D. Ansell, B. Thackray, K. S. Novoselov, A. K. Geim, A. V. Kabashin and A. N. Grigorenko, *Nat. Mater.*, 2013, **12**, 304-309.
14. L. C. Clark, Jr. and C. Lyons, *Ann. N. Y. Acad. Sci.*, 1962, **102**, 29-45.
15. A. Harper and M. R. Anderson, *Sensors*, 2010, **10**, 8248-8274.
16. L. L. Zhang, H. H. Cheng, H. M. Zhang and L. G. Qu, *Electrochim Acta*, 2012, **65**, 122-126.
17. M. B. Gholivand and M. Khodadadian, *Biosens. Bioelectron.*, 2014, **53**, 472-478.
18. H. H. Li, S. Q. Liu, Z. H. Dai, J. C. Bao and X. D. Yang, *Sensors*, 2009, **9**, 8547-8561.
19. A. K. Sarma, P. Vatsyayan, P. Goswami and S. D. Minteer, *Biosens. Bioelectron.*, 2009, **24**, 2313-2322.
20. Y. Q. Yang, A. M. Asiri, Z. W. Tang, D. Du and Y. H. Lin, *Mater. Today*, 2013, **16**, 365-373.
21. A. P. Pandey, K. P. Karande, M. P. More, S. G. Gattani and P. K. Deshmukh, *J. Biomed. Nanotechnol.*, 2014, **10**, 179-204.
22. E. K. Wujcik and C. N. Monty, *Wiley Interdiscip. Rev.-Nanomed. Nanobiotechnol.*, 2013, **5**, 233-249.
23. E. P. Bellido and J. M. Seminario, *J. Phys. Chem. C*, 2010, **114**, 22472-22477.
24. S. Zhu and T. Li, *ACS Nano*, 2014, **8**, 2864-2872.

25. G. Wohlfahrt, S. Witt, J. Hendle, D. Schomburg, H. M. Kalisz and H. J. Hecht, *Acta Crystallogr. D. Biol. Crystallogr.*, 1999, **55**, 969-977.
26. G. A. Kaminski, R. A. Friesner, J. Tirado-Rives and W. L. Jorgensen, *J. Phys. Chem. B*, 2001, **105**, 6474-6487.
27. H. J. C. Berendsen, J. P. M. Postma, W. F. van Gunsteren and J. Hermans, in *Intermolecular Forces*, ed. B. Pullman, D. Reidel Publishing Company, Dordrecht 1981, pp. 331–342.
28. U. Essmann, L. Perera, M. L. Berkowitz, T. Darden, H. Lee and L. G. Pedersen, *J. Chem. Phys.*, 1995, **103**, 8577-8593.
29. G. Bussi, D. Donadio and M. Parrinello, *J. Chem. Phys.*, 2007, **126**, 014101.
30. H. J. C. Berendsen, J. P. M. Postma, W. F. Vangunsteren, A. Dinola and J. R. Haak, *J. Chem. Phys.*, 1984, **81**, 3684-3690.
31. B. Hess, H. Bekker, H. J. C. Berendsen and J. G. E. M. Fraaije, *J. Comput. Chem.*, 1997, **18**, 1463-1472.
32. M. Parrinello and A. Rahman, *J. Appl. Phys.*, 1981, **52**, 7182-7190.
33. B. Hess, C. Kutzner, D. van der Spoel and E. Lindahl, *J. Chem. Theory Comput.*, 2008, **4**, 435-447.
34. D. Van der Spoel, E. Lindahl, B. Hess, G. Groenhof, A. E. Mark and H. J. C. Berendsen, *J. Comput. Chem.*, 2005, **26**, 1701-1718.
35. Y. Duan, C. Wu, S. Chowdhury, M. C. Lee, G. Xiong, W. Zhang, R. Yang, P. Cieplak, R. Luo, T. Lee, J. Caldwell, J. Wang and P. Kollman, *J. Comput. Chem.*, 2003, **24**, 1999-2012.
36. J. M. Wang, R. M. Wolf, J. W. Caldwell, P. A. Kollman and D. A. Case, *J. Comput. Chem.*, 2004, **25**, 1157-1174.
37. S. Nose, *J. Chem. Phys.*, 1984, **81**, 511-519.
38. W. G. Hoover, *Phys. Rev. A*, 1985, **31**, 1695–1697.
39. D. Porezag, T. Frauenheim, T. Kohler, G. Seifert and R. Kaschner, *Phys. Rev. B*, 1995, **51**, 12947-12957.
40. M. Elstner, D. Porezag, G. Jungnickel, J. Elsner, M. Haugk, T. Frauenheim, S. Suhai and G. Seifert, *Phys. Rev. B*, 1998, **58**, 7260-7268.
41. B. Aradi, B. Hourahine and T. Frauenheim, *J. Phys. Chem. A*, 2007, **111**, 5678-5684.

42. Y. Zhao and D. G. Truhlar, *Theor. Chem. Acc.*, 2008, **120**, 215-241.
43. E. Krieger, T. Darden, S. B. Nabuurs, A. Finkelstein and G. Vriend, *Proteins*, 2004, **57**, 678-683.
44. W. Humphrey, A. Dalke and K. Schulten, *J. Mol. Graph.*, 1996, **14**, 33-38.
45. Y. Wei, B. Wang, J. Wu, R. Yang and M. L. Dunn, *Nano Lett.*, 2013, **13**, 26-30.
46. D. B. Zhang, E. Akatyeva and T. Dumitrica, *Phys. Rev. Lett.*, 2011, **106**, 255503.
47. R. Kumar, V. M. Suresh, T. K. Maji and C. N. R. Rao, *Chem. Commun.*, 2014, **50**, 2015-2017.
48. W. F. Chen and L. F. Yan, *Nanoscale*, 2011, **3**, 3132-3137.
49. Y. Wang and Y. J. Yao, *Microchim. Acta*, 2012, **176**, 271-277.
50. M. Wooten, S. Karra, M. Zhang and W. Gorski, *Anal. Chem.*, 2014, **86**, 752-757.
51. J. Dudzik, W. C. Chang, A. M. Kannan, S. Filipek, S. Viswanathan, P. Li, V. Renugopalakrishnan and G. F. Audette, *Biofabrication*, 2013, **5**, 035009.
52. Y. Y. Yu, Z. G. Chen, S. J. He, B. B. Zhang, X. C. Li and M. C. Yao, *Biosens. Bioelectron.*, 2014, **52**, 147-152.
53. W. Grosse, J. Champavert, S. Gambhir, G. G. Wallace and S. E. Moulton, *Carbon*, 2013, **61**, 467-475.
54. A. Ueda, D. Kato, R. Kurita, T. Kamata, H. Inokuchi, S. Umemura, S. Hirono and O. Niwa, *J. Am. Chem. Soc.*, 2011, **133**, 4840-4846.
55. Z. M. Luo, X. B. Ma, D. L. Yang, L. H. Yuwen, X. R. Zhu, L. X. Weng and L. H. Wang, *Carbon*, 2013, **57**, 470-476.
56. Y. Chen, F. Guo, A. Jachak, S. P. Kim, D. Datta, J. Liu, I. Kulaots, C. Vaslet, H. D. Jang, J. Huang, A. Kane, V. B. Shenoy and R. H. Hurt, *Nano Lett.*, 2012, **12**, 1996-2002.
57. G. Shi, Y. Ding and H. Fang, *J. Comput. Chem.*, 2012, **33**, 1328-1337.

Figure Legends

Figure 1 Crystal structure of GOx dimer. (a) The secondary structure. (b) The molecular surface of GOx dimer showing an entrance to the active site from both sides of GOx dimer. The cofactor, FAD (flavin adenine dinucleotide), is shown as van der Waals spheres.

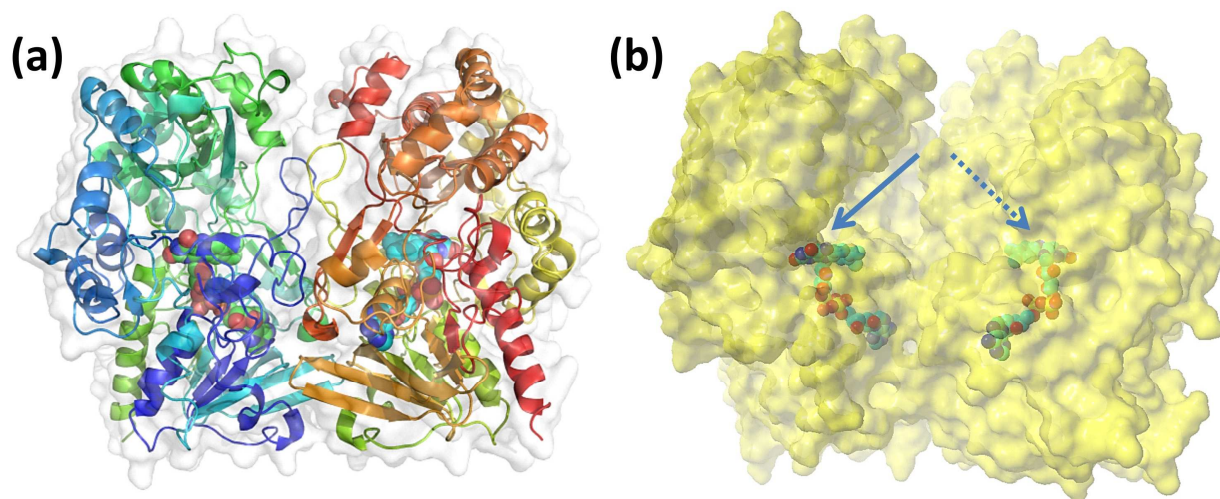


Figure 2 Structures of GOx dimer with four unconnected graphene sheets. (a) The positions of graphene sheets after a short equilibration procedure; (b) after 2 ns of MD simulation; (c) after 100 ns of MD simulation.

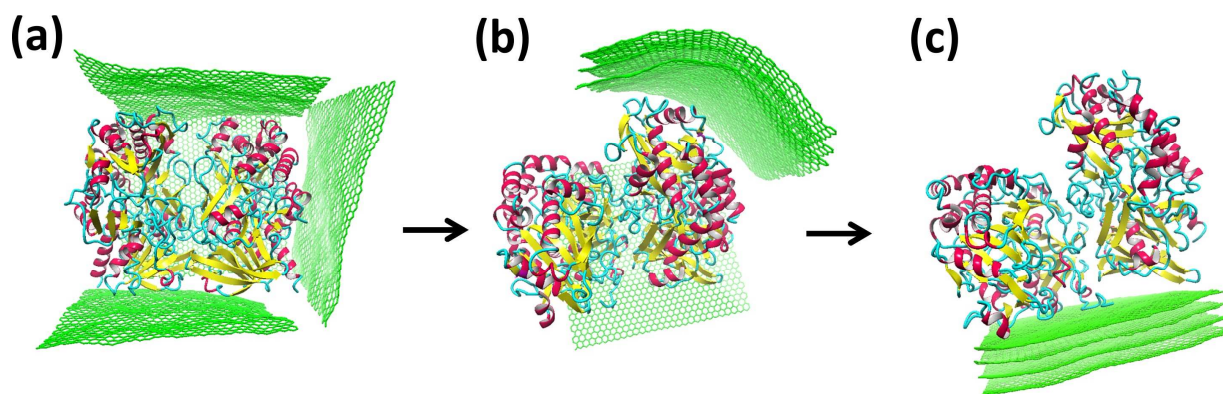


Figure 3 Structures of GOx dimer in boxlike graphene with different linker widths between graphene sheets. (a) Linker width 0.7 nm (three benzene rings) - Box1. (b) 1.9 nm - Box2. (c) 3.8 nm - Box3. (d) 7.0 nm (equal to the size of the sheet) - Box4. (e) Box4 mapped with graphene surface curvature; blue – lowest curvature, red – highest curvature. (f) Overlapping graphene sheets in Box4 model. A view from a corner showing a tightly curved graphene.

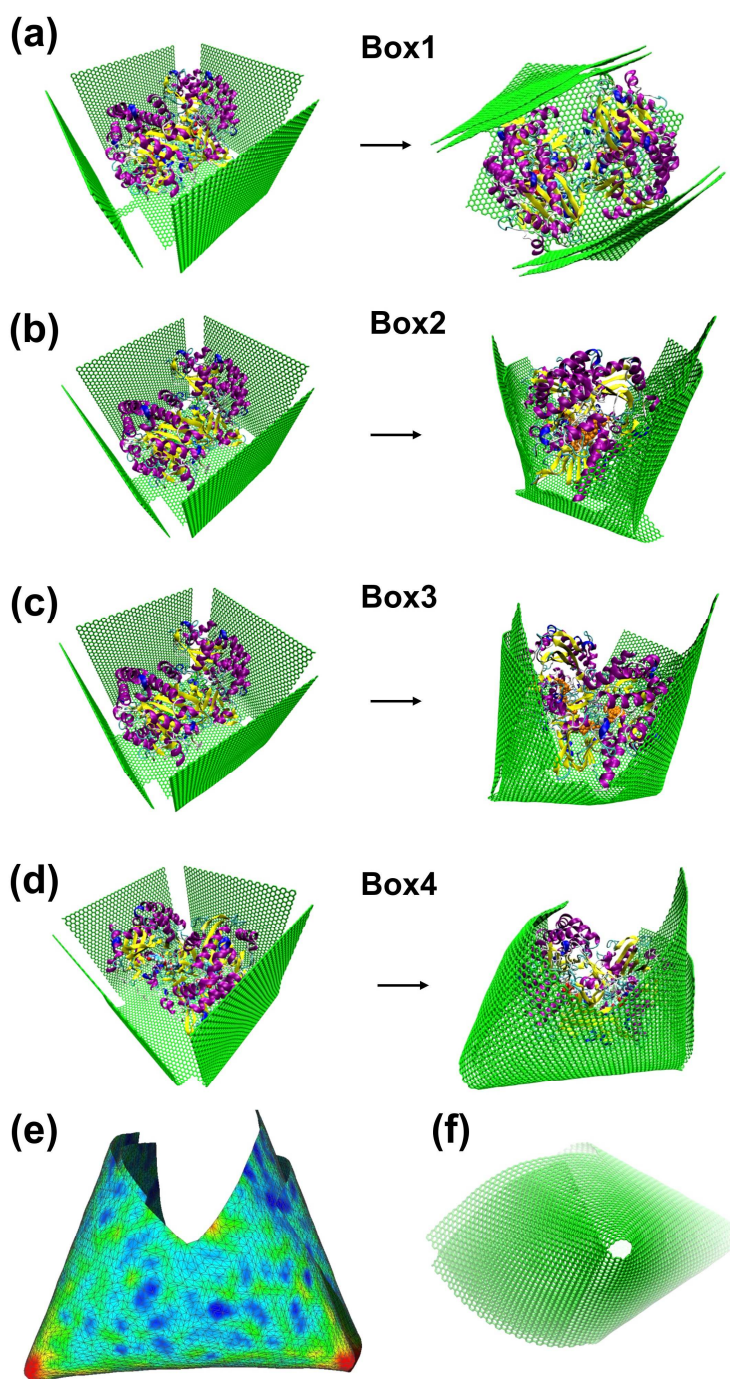


Figure 4 Location of flavin rings of cofactor FAD in the active site of GOx. Catalytic histidine residues are coloured in purple. (a) Oxidized form (in orange) and reduced form (in green) of FAD. (b) Binding of flavin group of FAD in Box1 model after 100 ns of MD simulation. (c) Displaced position of the flavin group in Box4 model after 100 ns of MD simulation.

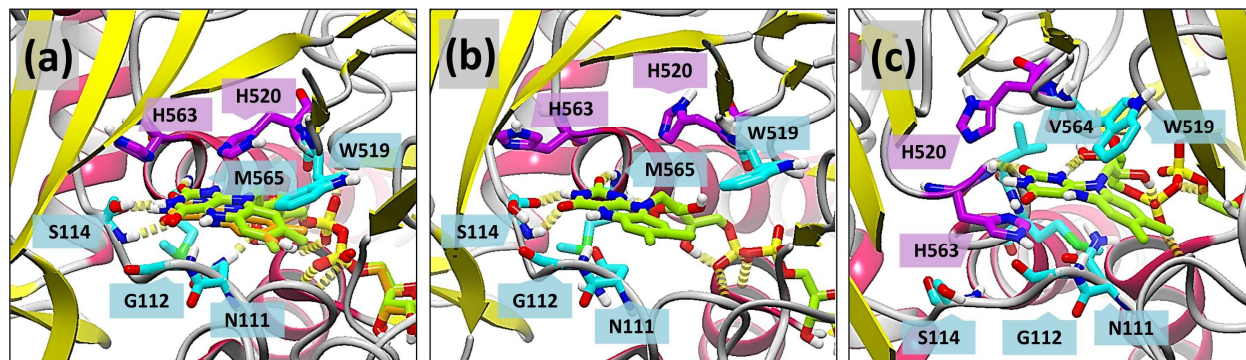
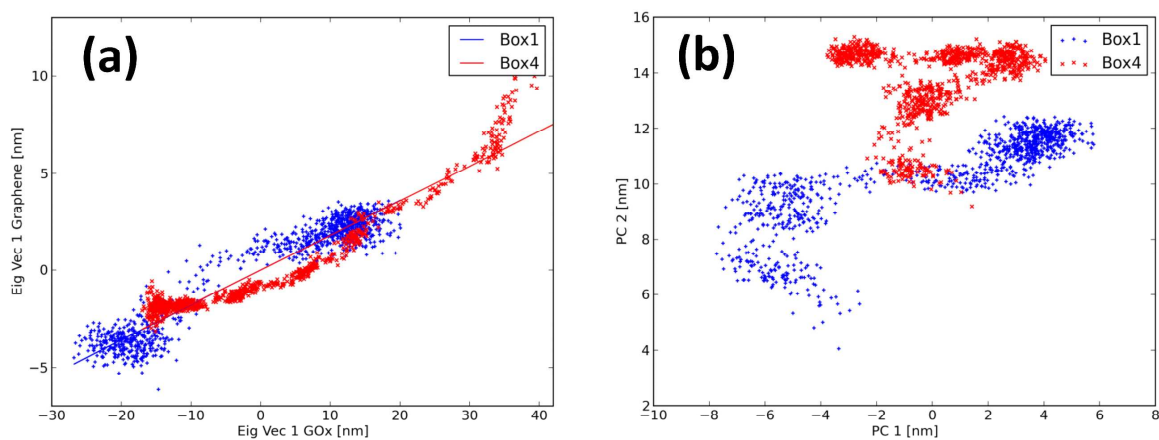


Figure 5 Principal Component Analysis of MD simulations of Box1 and Box4 models. (a) A correlation between principal components of GOx dimer and graphene. (b) Distinct conformational changes of GOx dimer in Box1 and Box4.



Tables

Table 1 Comparison of properties of GOx complexes. Structures of Stack, Box1 and Box4 models after 100 ns MD simulation in explicit water environment. Numbers in bold indicate extreme values.

Complex	Crystal	Stack	Box1	Box4
GOx-GOx centre distance	3.85 nm	4.10 nm	4.14 nm	3.24 nm
GOx-GOx contact area	22.9 nm ²	20.7 nm ²	26.0 nm ²	77.9 nm²
FAD-graphene closest distance	---	---	1.86 nm	1.85 nm
GOx-graphene contact area	---	31 nm ²	138 nm ²	204 nm²